Article

Anti-Corrosion Performance of Polyaniline Coated Basalt Rockwool Wastes/Epoxy Resin Coatings

Zhiqiang Fang [1], Guoqing Wang [1,*], Yangkai Xiong [1], Jiang Li [2], Yu Yang [1], Lei Huang [1], Peiqing Wang [3], Jianhe Liao [1] and Aimin Wang [1]

[1] State Key Laboratory of Marine Resource Utilization in South China Sea, School of Materials Science and Engineering, Hainan University, No. 58, Renmin Avenue, Haikou 570228, China; 15754332338@163.com (Z.F.); x64880030@163.com (Y.X.); Yangyu20210224@163.com (Y.Y.); HL1842251332@163.com (L.H.); 990359@hainanu.edu.cn (J.L.); aimwang@163.com (A.W.)

[2] Industrial & Manufacturing Engineering, College of Engineering, Florida State University, Tallahassee, FL 32306, USA; jl16u@my.fsu.edu

[3] Sichuan Sunvea New Materials Co., Ltd., Guangan 638500, China; wangpeiqing@sunvea.com

* Correspondence: wangguoqing@hainanu.edu.cn

Abstract: Basalt rockwool wastes with large output, which are toxic and require expensive environmental treatment, are produced during the production of rock wool. Hence, it is urgent to find an effective method to reuse these materials. In this study, polyaniline (PANI)-coated basalt rockwool wastes (BRWs) were prepared as fillers to serve in coatings for the anticorrosion study. Results show that the PANI-coated BRW (PANI@BRW) had enhanced dispersion stability in several conventional solvents and improved the anticorrosion performance of the epoxy resin coating. A high protection efficiency of 97.7% could be obtained from the coating with 5% fillers after immersion for 30 days. This study not only provides a promising method of solving the issues caused by BRW, but also turns these wastes into valuable substances.

Keywords: basalt rockwool waste; inorganic fillers; polyaniline; epoxy resin; anti-corrosion; protection efficiency

1. Introduction

Basalt rockwool has been widely used as a thermal insulating filler in building materials [1,2]. As demands increase, the waste generated during production also increases. It is reported that the total output of the basalt rockwool wastes (BRWs) produced by the EU has already exceeded 2.3 million tons per year and continues to grow [3]. The large amount of BRW with ammonia smell causes environmental issues and increases the cost of post-treatments.

In recent years, basalt scales, as inorganic pigments, have widely served in anti-corrosion coatings [4,5]. They can effectively protect the metal matrix from corrosion for a long time due to the "labyrinth effect", which can hinder or delay the intrusion of corrosive factors such as oxygen and water [4,6–8]. BRW is similar in chemical composition and size to the basalt scale. A promising method to reduce the impacts and improve the value of BRW is to use them as fillers in anti-corrosion coatings. In addition, with the BRWs as fillers, the coatings do not contain metals such as zinc and aluminum. They can be implemented underwater and are suggested to serve as a primer for marine antifouling coatings.

Polyaniline (PANI) has attracted a great deal of attention in the field of metal anti-corrosion, antistatic materials, and electronic chemicals [9–11]. It has a low monomer price, easy fabrication, good environmental stability and unique oxidation–reduction with a catalytic passivation mechanism [12–18]. In addition, it is expected to be applied to almost all metal surfaces using the appropriate technology due to its relatively low impact on human health and the environment.

Even though BRWs and PANI show advantages in anticorrosion coatings, they also have their own limits. For BRW, as an inorganic material, the poor compatibility with epoxy resin reduces the quality of coatings. Moreover, owing to the amino group on the surface of BRW, the epoxy resin is cured immediately and cannot be implemented. PANI has high crystallinity and is difficult to dissolve in normal solvents due to the rigid benzene structure that greatly restricts its application in coatings [19,20].

In this paper, PANI-coated BRW was prepared and used as a filler in epoxy resin coatings. The PANI prevents the BRW from directly contacting with the epoxy resin that improves the compatibility between them. Furthermore, the passivation effect of PANI on the metal and the physical barrier effect of the BRW will significantly enhance the anti-corrosion performance of the composite coatings. Therefore, the existence of these components in the coating makes it possible to protect the metals from corrosion. Due to the non-metal elements included, this coating is especially applicable to surfaces that are exposed to a marine environment, such as the surfaces of boats and offshore platforms. Good anti-corrosion performance will greatly promote the application and increase the worth of BRWs.

2. Experimental

2.1. Materials

Aniline (An), ammonium persulfate (APS), phosphoric acid (H_3PO_4), *N*-methylpyrrolidone (NMP), *N*, *N*-dimethylformamide (DMF), and ethanol were purchased from Sinopharm Chemical Reagent Co., Ltd. (Beijing, China). Basalt rockwool waste (BRW) was provided by Sichuan QianYi Composite Material Co., Ltd. (Guangan, China). The as-purchased materials are shown in Figure 1a. The uncoated BRW has a short fiber shape, while its surface is smooth and delicate. EDS analysis demonstrates that the surface of the BRW is mainly made up of silicon and oxygen elements as shown in Figure 1b–d. Epoxy resin (ER, E51), polyamide curing agent (650), *n*-butanol, and xylene were purchased from Sanmu Chemical Co., Ltd. (Yixing, China). Deionized water was made in our own laboratory. All reagents were used as received.
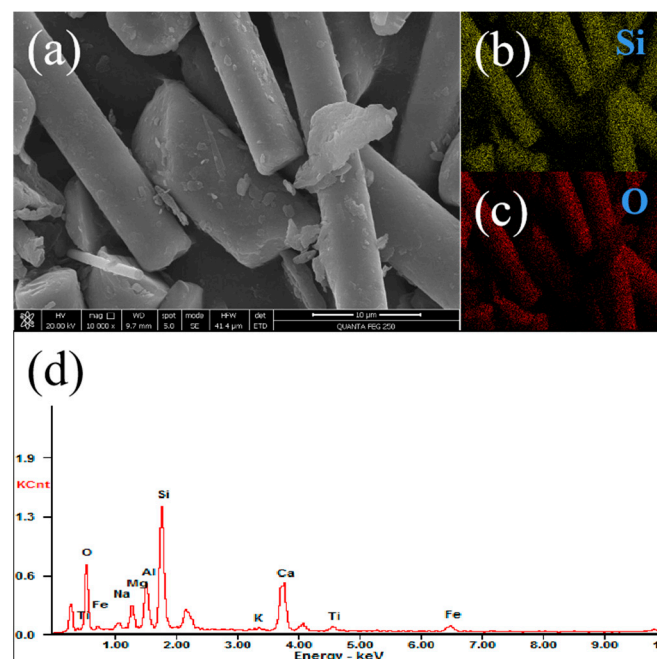

Figure 1. (**a**) SEM image, (**b**,**c**) elemental mapping, and (**d**) EDS spectrum of basalt rock waste (BRW).

2.2. Method

2.2.1. Synthesis of PANI and PANI@BRW

Initially, 2 g of aniline and 6 g of BRW were mixed with 10 mL deionized water and kept in an ice-water bath for 15 min, and then 20 mL of 0.5 mol/L H_3PO_4 was added, as shown in Figure 2 [15]. After continuous stirring for 30 min, the APS/H_3PO_4 solution, which was prepared in advance by dissolving 5.8 g APS in 60 mL H_3PO_4, was slowly added into the mixture [4]. The mixture was stirred for 3 h and then kept for 24 h. Finally, the mixed solution was filtrated and the obtained particles were washed with deionized water and ethanol five times. In the end, the dark green PANI-coated BRW (PANI@BRW) was obtained through filtration and dried in a vacuum oven at 60 °C. With the same steps, pure PANI was synthesized without the addition of BRW and used as a control.
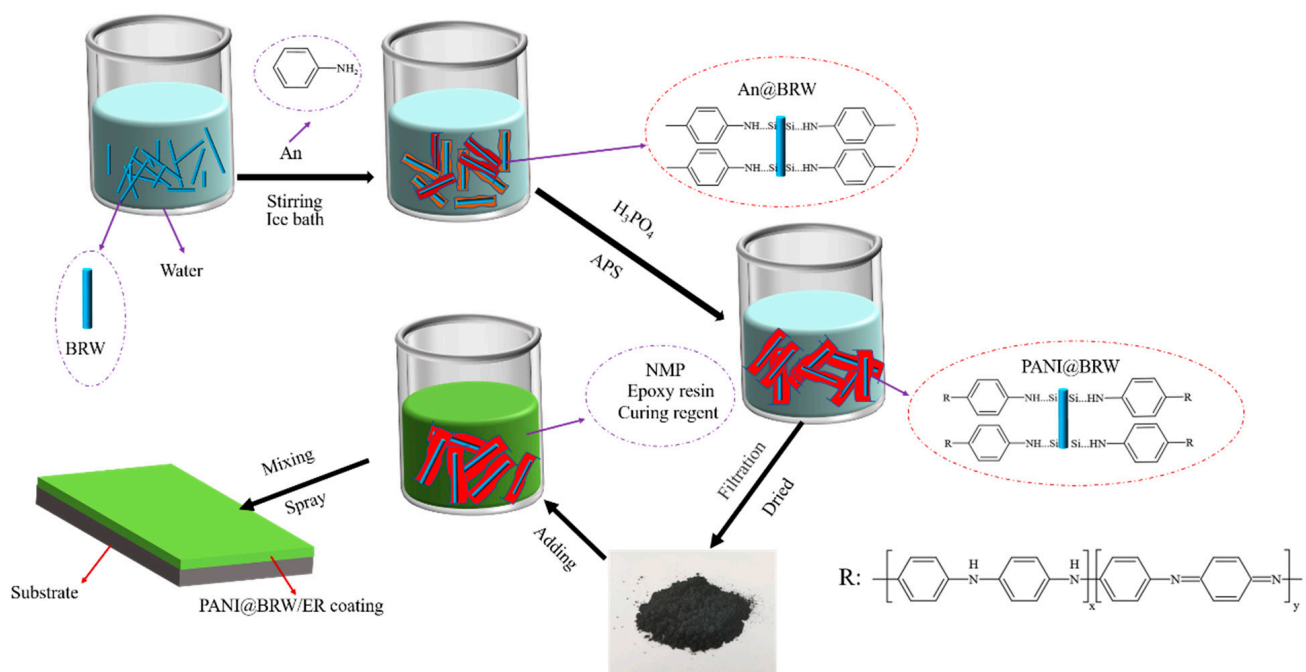

Figure 2. Preparation of polyaniline-coated basalt rockwool wastes/epoxy resin (PANI@BRW/ER) coating.

2.2.2. Preparation of Coatings

To fabricate PANI-coated BRW/epoxy resin (PANI@BRW/ER) coatings, 10 g epoxy resin, 10 g curing agent, and PANI@BRW were added to the NMP and completely blended through ultrasonic dispersion and stirring. To evaluate the effect of PANI@BRW fillers on the properties of coatings, the PANI@BRW/ER coatings with different amounts of fillers (0.25 g, 0.5 g, and 0.75 g) were fabricated and marked as PANI@BRW/ER1, PANI@BRW/ER2, and PANI@BRW/ER3, respectively. In addition, pure epoxy resin (ER) coating, PANI/epoxy resin (PANI/ER) coating, and BRW/epoxy resin (BRW/ER) coating were prepared as controls. The paint was sprayed on a substrate of surface-treated carbon steel with a size of 1 cm × 1 cm. After 7 days at room temperature, fully cured coatings were obtained.

2.3. Characterization

2.3.1. Characterization of PANI and PANI@BRW

To determine the structure and properties of the fillers, a field-emission scanning electron microscope (FESEM, Verios G4 UC, Thermo Fisher Scientific Brno Co., Ltd., Waltham, MA, USA) was used to observe the surface morphology of the samples. X-ray diffractometer (XRD, Rigaku Company, Akishima, Japan) was used to study the crystalline properties of polyaniline and composites with the diffraction angle set from 10° to 80°. Fourier-transform infrared spectroscopy (FT-IR, Bruker, Karlsruhe, Germany) was implemented in

testing the structure of polyaniline and composites, and the spectrum was collected within the wavenumber range of 4000–400 cm^{-1}. After ultrasonically dispersing the samples in different solvents (water, ethanol, NMP, and DMF), respectively, the results were compared to show their dispersion stability. Thermogravimetric analysis (TGA, NETZSCH, Selb, Germany) was used to characterize the thermal stability of the samples and tested from room temperature (RT) to 800 °C.

2.3.2. Characterization of Coatings

A salt spray test was used to evaluate the anti-corrosion performance of the coatings. Tests were implemented in a salt spray chamber with a NaCl concentration of 5 ± 0.5 wt.% and a pH value of 6.5–7.0 [21].

By immersing the coating samples in 3.5 wt.% NaCl solution, the electrochemical signal changes under different saturation times were recorded. A three-electrode system was employed to characterize the anti-corrosion performance of the coatings using the DH7000 electrochemical workstation. The open circuit potential (OCP) test was carried out to study the changes in the corrosion potential of the coatings. EIS was measured to analyze the corrosion resistance of the coatings with a working frequency ranging from 10^{-2} to 10^5 Hz and an amplitude of 10 mV. The ZView software was used to record Nyquist and Bode plots. In addition, the polarization curve test of the coatings was performed before and after immersion for 30 days with a scanning voltage in the range of ±0.25 V (vs. OCP), a sweep rate of 1 mV/s, and the test conditions required for when the open circuit potential remained stable.

The coating adhesion was measured according to the pull-off method in accordance with the ASTM D4541-2009 by PosiTest Pull-Off Adhesion Tester (DeFelsko Corporation, Ogdensburg, NY, USA) [15].

3. Results and Discussion

3.1. Characterization of PANI and PANI@BRW

3.1.1. Micromorphology Analysis

Figure 3 shows the FESEM images of PANI and PANI@BRW. Figure 3a shows that the as-prepared PANI powders aggregated to form clusters. With the addition of BRW, the PANI was coated on the surface of BRW, as shown in Figure 3b. The layer of PANI was designed to avoid direct contact between the inorganic material and the organic solvent, and it was expected to improve the dispersion stability of the composites in the different solvents.
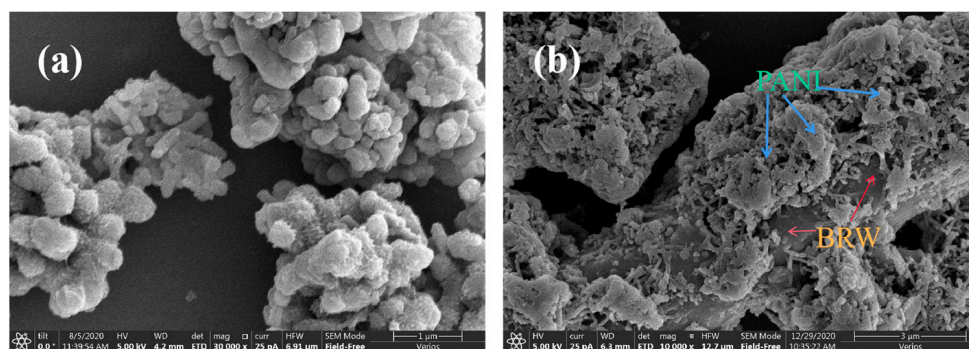

Figure 3. SEM images of (**a**) PANI, (**b**) PANI@BRW (mass ratio, An/BRW = 1:3).

3.1.2. Microstructure Characterization

The FT-IR spectra of BRW, PANI, and PANI@BRW are shown in Figure 4. For the spectrum of BRW, there is a broad peak near 1028 cm^{-1}, which represents the Si-OH of BRW. The main characteristic peaks of the PANI at 1564 cm^{-1} and 1483 cm^{-1} relate to C=C tensile vibrations which are attributed to the quinone ring and the benzene ring in the polyaniline segment, respectively [22]. The peaks at 1300 cm^{-1} and 1245 cm^{-1} correspond

to C-N stretching vibrations of the benzene ring, respectively [18]. The peak at 1111 cm^{-1} is attributed to the quinoid unit of polyaniline. The peaks of these quinone rings and benzene rings prove that the polyaniline exists in the form of emeraldine salt [23]. The spectrum of PANI@BRW is similar to that of PANI. However, the peaks at 1111 cm^{-1} and 1245 cm^{-1} disappear due to the overlap with the peak of Si-OH on the BRW surface. The peaks shift from 1564 cm^{-1} and 1483 cm^{-1} to 1588 and 1499 cm^{-1}, which indicates the interaction between the PANI and the BRW. It may be attributed to a large number of hydrogen bonds that are formed between the polyaniline and the basalt rockwool waste [4,24].
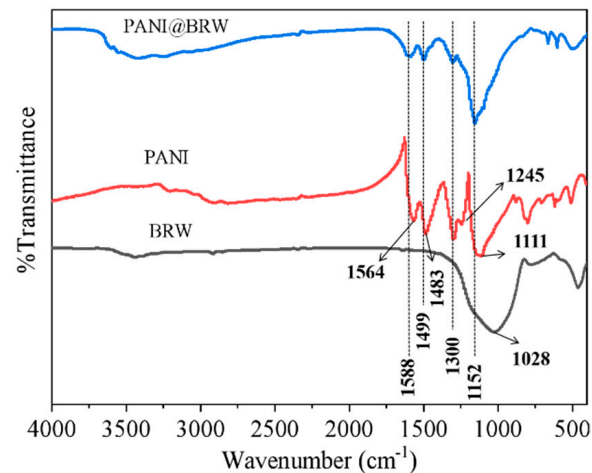

Figure 4. Fourier-transform infrared (FT-IR) spectra of BRW, PANI, and PANI@BRW.

3.1.3. X-ray Diffraction Analysis

In order to verify the changes of PANI in terms of crystallinity, X-ray diffraction (XRD) analysis was performed on BRW, PANI, and PANI@BRW, and the results are presented in Figure 5. The diffraction pattern of BRW shows a broad peak in the range of 10°–30°, which behaves as a clear amorphous phase. The pattern of PANI has sharper diffraction peaks at 15.15°, 20.48°, and 25.50° that correspond to its (011), (100), and (110) crystal planes, respectively [16,25,26]. With the introduction of BRW, the intensity of these peaks was significantly weakened, which indicates that the crystallinity of PANI was reduced due to the interaction between PANI and BRW.
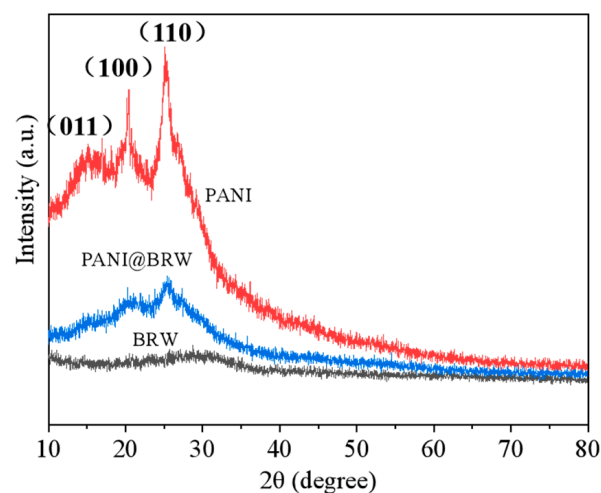

Figure 5. X-ray diffraction (XRD) patterns of BRW, PANI, and PANI@BRW.

3.1.4. Stability of Samples in Different Solvents

The dispersion stability of fillers in solvents is an important parameter of organic coatings. As shown in Figure 6, BRW, PANI, and PANI@BRW, arranged from left to right, were dispersed in different polar solvents including water, absolute ethanol, DMF, and NMP, respectively. The samples were dispersed by ultrasound for 30 min and then left to stand still to observe the stability of the dispersions. The results show that, immediately after dispersion, all samples could be uniformly dispersed in the four solvents. After 1 day, the BRW completely deposited in all four solvents but the PANI remained well-dispersed in two solvents (DMF and NMP). PANI@BRW was able to distribute stably in three solvents except for water, even after 7 days. This indicates that the PANI layer improved the dispersion stability of the BRW in the solvents. Comparing to PANI, the better stability of PANI@BRW may be due to the interaction between PANI and BRW, which decreases the crystallinity of PANI. The good dispersion stability makes PANI@BRW a more likely candidate as a filler in epoxy resin coatings.
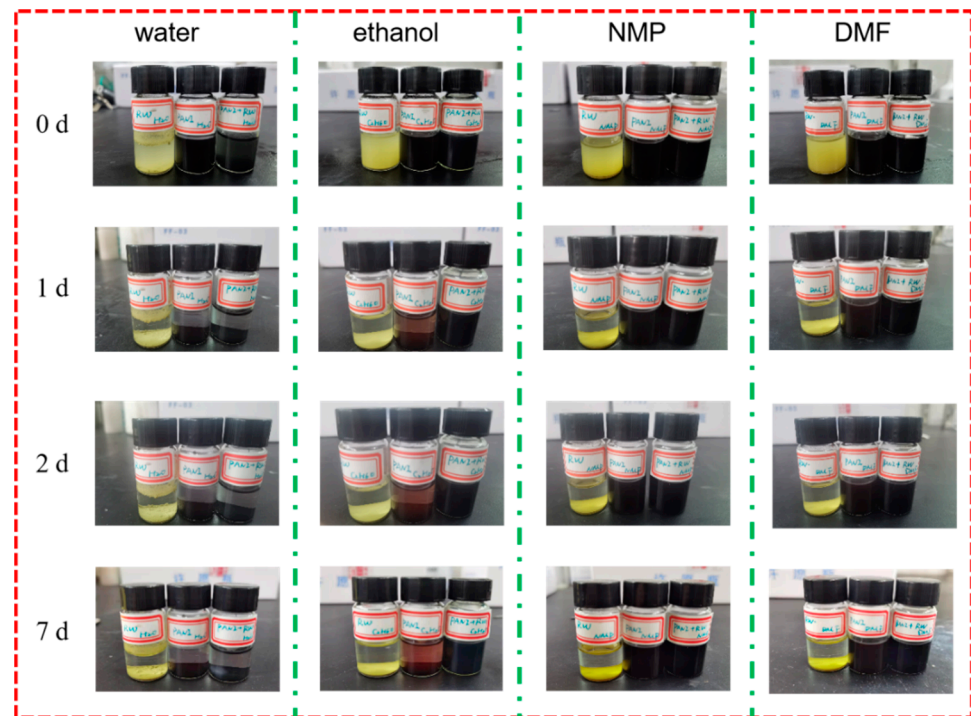

Figure 6. Dispersion stability of BRW, PANI, and PANI@BRW in different solvents (BRW, PANI, and PANI@BRW are arranged from left to right in each image).

3.1.5. Thermogravimetric Analysis

Figure 7 shows the thermogravimetric analysis of BRW, PANI, and PANI@BRW. The raw BRW lost 1.4% of its weight during the entire heating process, which is attributed to the volatilization of water in the material [16]. For pure PANI, except for the volatilization of water at about 150 °C, the main weight loss started from approximately 300 °C as a result of the decomposition of PANI. However, the starting decomposition temperature of PANI@BRW was nearly 350 °C. This may be due to the strong interaction between PANI and BRW [4]. The results illustrate that the thermal stability of the PANI@BRW was improved. The differences between the curves can also testify that the mass ratio of PANI to BRW in the composite is approximately 1:3.
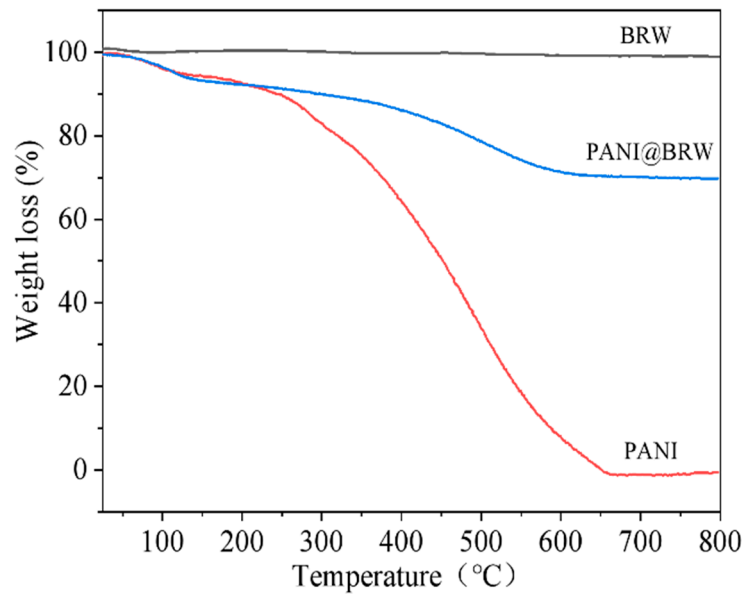
Figure 7. Thermogravimetric analysis (TGA) diagrams of BRW, PANI, and PANI@BRW.

3.2. Characterization of the Coatings

3.2.1. Salt Spray Test

The salt spray test serves as an accelerated corrosion test method for laboratory research on the anti-corrosion performance of coatings. It was conducted to detect the corrosion protective efficiency of the coatings and to predict their service life in practical applications. The anti-corrosion performance of steel sheets with different coatings before and after salt spray tests are summarized in Figure 8. The results show that sheets with ER coating and BRW/ER coatings started to blister on the surface in less than 15 days while there were no obvious corrosion products observed on the sheets with PANI/ER and PANI@BRW/ER coatings. After 40 days, the sheets with the PANI@BRW/ER2 and PANI@BRW/ER3 coatings were still in good condition, without corrosion. These results conclude that the PANI@BRW can effectively improve the anti-corrosion performance of ER coatings.

3.2.2. Open Circuit Potential (OCP)

The OCP values of the different samples are shown in Figure 9. Compared with the ER coating, the OCP value of the BRW/ER coating was even lower. This can be attributed to the inorganic powders, which have poor compatibility with epoxy resin and increase the defects in the coating. The defects provide pathways for water, oxygen, and ions to penetrate the coating and reach the surface of the substrate. The OCP value of the ER and BRW/ER coatings changed greatly at the beginning as the substrates were corroded and reaction products were generated [27]. Meanwhile, due to the presence of PANI, the PANI/ER and PANI@BRW/ER coatings showed high potential and the OCP values fluctuated little. This indicates that during the immersion stage, the polyaniline in the coatings passivated the carbon steel and resulted in a stable interface between the coating and the substrate [9].
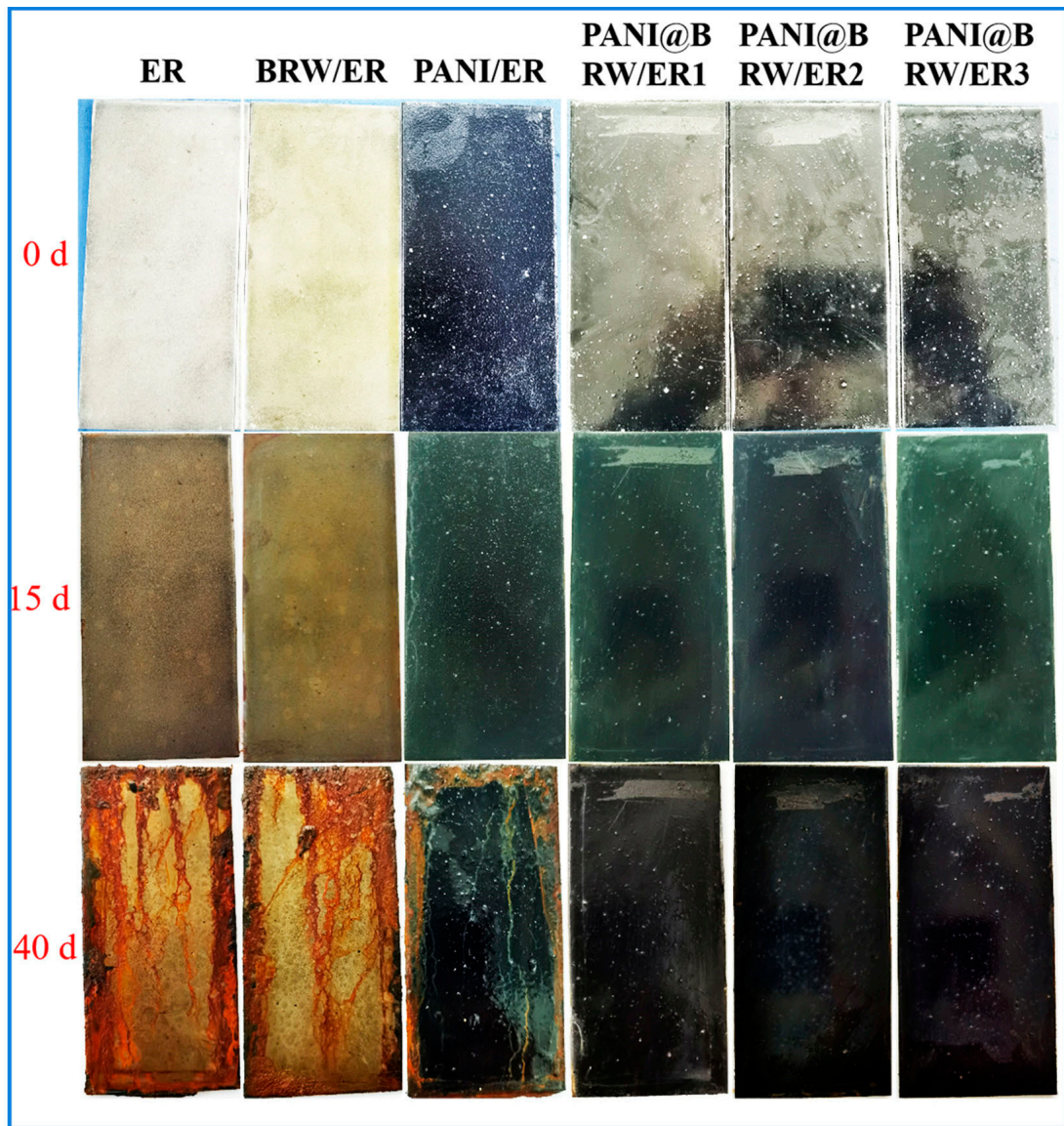
Figure 8. Images of ER, BRW/ER, PANI/ER, PANI@BRW/ER1, PANI@BRW/ER2, and PANI@BRW/ER3 coatings subjected to salt spray test after 0 d, 15 d, and 40 d, respectively.
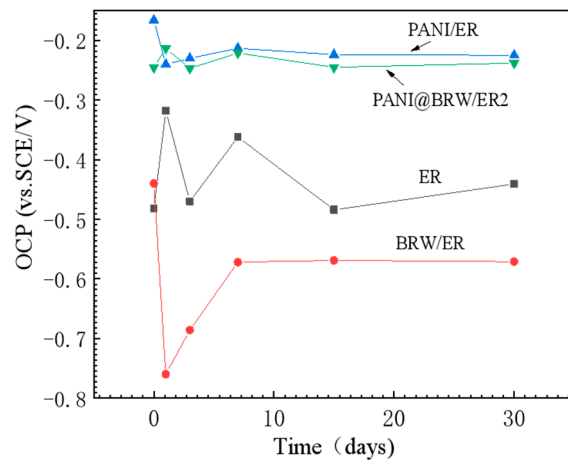

Figure 9. Open circuit potential (OCP) of ER, BRW/ER, PANI/ER, and PANI@BRW/ER coatings.

3.2.3. Polarization Curve Test

To better explore the anti-corrosion performance of the PANI@BRW/ER coatings, the Tafel polarization curve of the coatings was recorded Bare carbon steel (CS) samples with ER, BRW/ER, PANI/ER, PANI@BRW/ER1, PANI@BRW/ER2, and PANI@BRW/ER3 coatings were immersed in 3.5% NaCl solution for 30 days and the polarization curve measurements before and after immersion were carried out as shown in Figure 10. The protection efficiency (*PE*) of the coatings is used to directly exhibit the anti-corrosion performance of different coatings [28–30]:

$$PE = \frac{i_{corr-cs} - i_{corr-coating}}{i_{corr-cs}} \times 100\% \tag{1}$$

where $i_{corr\text{-}cs}$ and $i_{corr\text{-}coating}$ represent the corrosion current density of uncoated and coated carbon steel, respectively. These two parameters can be obtained through the Tafel extrapolation. The corresponding values are shown in Table 1.
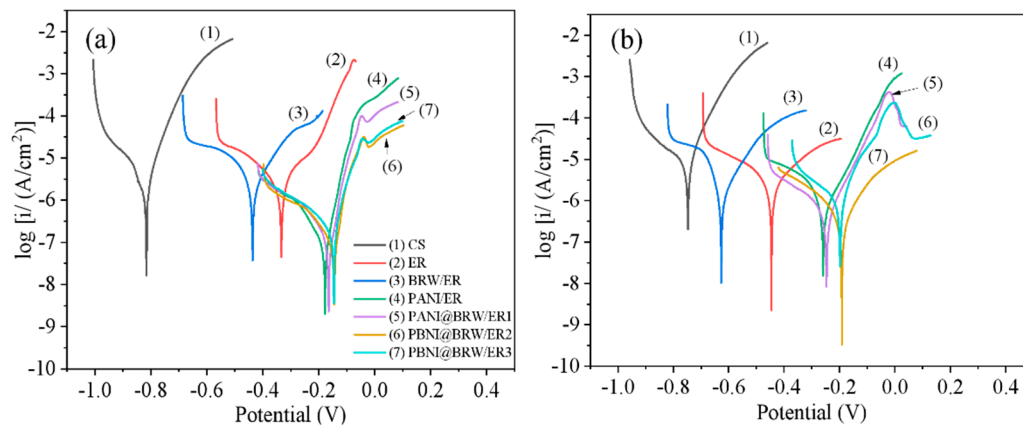

Figure 10. Tafel polarization curve for the coatings before (**a**) and after (**b**) immersion.

Table 1. The corrosion current density (i_{corr}), corrosion potential (E_{corr}), and protection efficiency (*PE*) of different coatings.

Sample	$i_{corr} \times 10^{-6}$ (A/cm^2)	E_{corr} (mV)	*PE* (%)	$i_{corr} \times 10^{-6}$ (A/cm^2)	E_{corr} (mV)	*PE* (%)
		0 d			30 d	
CS	3.0420	−810	-	2.1140	−744	29.5
ER	0.7824	−322	74.3	0.7223	−445	76.3
BRW/ER	1.0710	−434	64.8	0.8350	−630	72.6
PANI/ER	0.0367	−174	98.8	0.4687	−258	84.6
PANI@BRW/ER1	0.0424	−159	98.6	0.1563	−227	94.9
PANI@BRW/ER2	0.0351	−142	98.8	0.0688	−189	97.7
PANI@BRW/ER3	0.0497	−144	98.4	0.1835	−196	94.0

As shown in Figure 10a, the corrosion potential (E_{corr}) of the bare carbon steel was the most negative and the i_{corr} was the largest when the substrate was in an unprotected state. Besides, at the initial stage of immersion, the cured epoxy resin ensured that the ER and BRW/ER coatings provided a certain barrier effect, while the coatings with PANI and PANI@BRW had higher E_{corr}. Moreover, the cathode and anode branches of the polarization curve shifted significantly to the direction of lower i_{corr} relative to neat carbon steel [31–34]. These shifts are due to the combination of polyaniline and basalt rockwool waste. Without immersion, the *PE* values of the PANI/ER and PANI@BRW/ER coatings were higher than 98%, indicating that they possessed excellent corrosion resistance. After being immersed for 30 days (Figure 10b), the samples (CS, ER coating, and BRW/ER coating) displayed higher *PE*s than those before immersion. This is because of the corrosion products that formed on the surface of the substrates and protected the substrates from

further corrosion. The *PE* of the PANI/ER-coated sample dropped to 84.6% because the corrosive factors penetrated the coating during the immersion process and local corrosion occurred on the substrate. However, the polyaniline emeraldine salt in the intermediate oxidation state turned Fe to Fe^{2+}, obtaining reduced polyaniline. Subsequently, with the entry of dissolved oxygen, the further oxidation of the Fe^{2+} led to the formation of the Fe_2O_3 passive layer [28,35]. However, the *PE* of all the PANI@BRW/ER coatings was still larger than 94%, which indicates the improvement of the corrosion resistance compared to other coatings. Among all these samples, the PANI@BRW/ER2 coating showed the best protection efficiency.

3.2.4. Electrochemical Impedance Spectroscopy (EIS)

Electrochemical impedance spectroscopy (EIS) was used to detect the electrochemical characteristics of ER, BRW/ER, PANI/ER, PANI@BRW/ER1, PANI@BRW/ER2, and PANI@BRW/ER3 coatings [36]. The Bode plots and Nyquist plots were obtained from the coatings which were immersed in 3.5% NaCl solution for 0 h, 72 h, and 168 h. As shown in Figure 11, the Bode diagrams reveal the relationship between the impedance modulus and the frequency [37]. Correspondingly, the Nyquist plots describe the functional relationship between the real part and the imaginary part of the impedance [38].

In the Bode plots, the impedance modulus value at a frequency of 0.01 (i.e., 0.01 Hz) was used to evaluate the corrosion resistance of the coating, which is marked as $|Z|_{0.01}$. As shown in Figure 11, at 0 h, the result in the Bode plot (Figure 11a) shows that the $|Z|_{0.01}$ values of the PANI/ER and PANI@BRW/ER coatings were much higher than those of the ER and BRW/ER coatings. The $|Z|_{0.01}$ of the PANI@BRW/ER2 coating was 8.03×10^6 Ω cm^2, while that for the pure epoxy coating was only 8.7×10^3 Ω cm^2. On the Nyquist chart [37] (Figure 11b), PANI@BRW/ER2 and PANI@BRW/ER3 exhibit a complete semicircle. However, the BRW/ER coating exhibits a lower $|Z|_{0.01}$ than the pure epoxy. The results clearly show that the addition of PANI@BRW improved the corrosion resistance of the ER coating.

When all samples were immersed for 72 h, the $|Z|_{0.01}$ values were reduced, as shown in Figure 11c,d, but the resistance of the PANI@BRW/ER coating did not decrease significantly, which can be concluded from the slight decrease in the radius of the semicircle. However, the resistance of the PANI/ER coating dropped below those of the ER and BRW/ER coatings, which can be ascribed to water and ions that penetrated the coating. For the ER and BRW/ER coatings, the substrates were corroded on the surface and the corrosion products were generated. Therefore, the impedance of ER and BRW/ER coatings increased instead of decreasing.

After the coating was soaked for 168 h, the EIS was conducted on the coatings, and the results are shown in Figure 11e,f. The $|Z|_{0.01}$ of PANI/ER and PANI@BRW/ER coatings still maintained a relatively high impedance and the PANI@BRW/ER2 coating had the highest impedance value. This indicates that a larger amount of PANI@BRW may be beneficial to the anti-corrosion performance, but that an excessive amount may lead to an increase of defects in the coating. Here, the coating with 5% PANI@BRW achieved the best anti-corrosion performance.
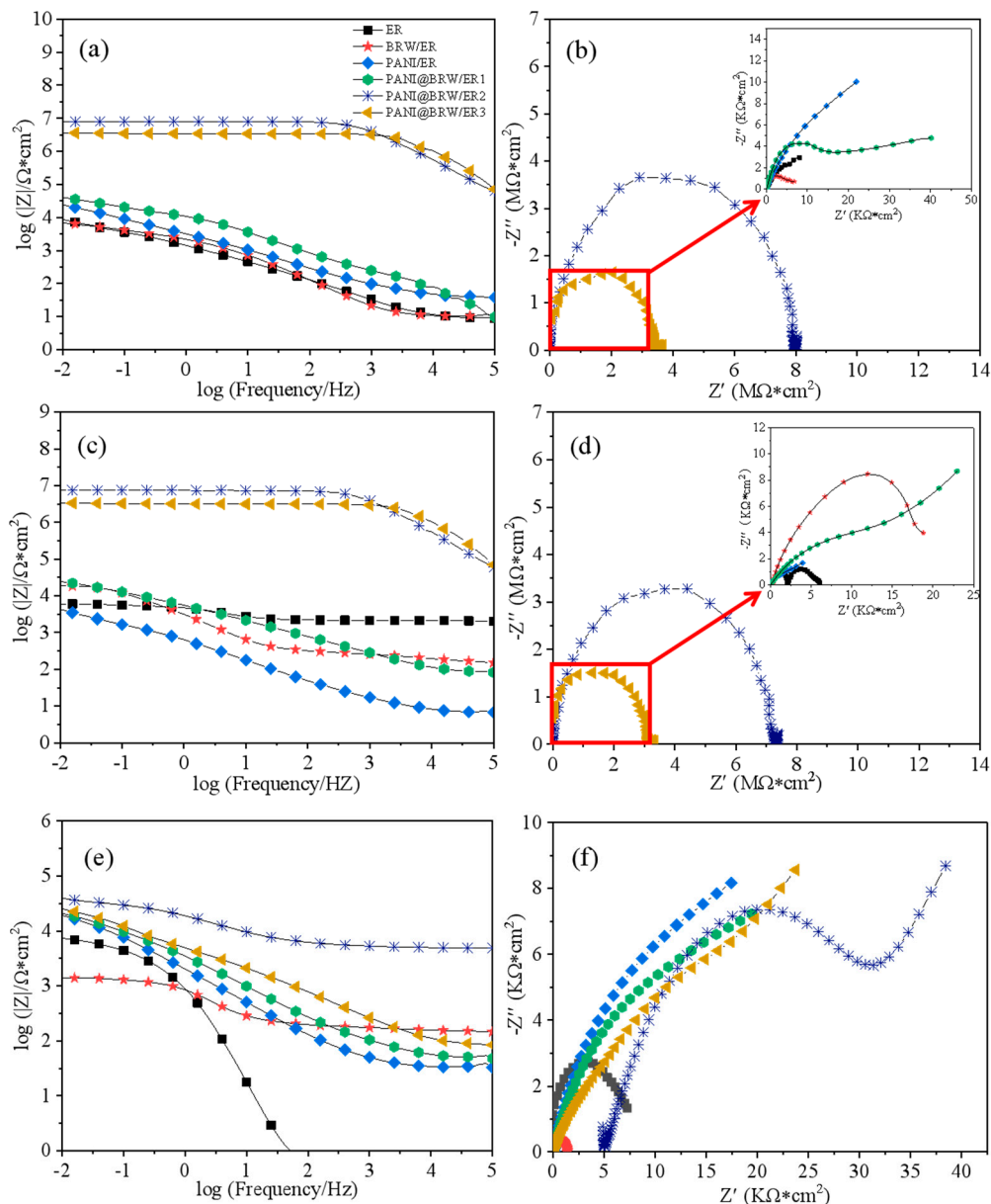
Figure 11. Bode plots and Nyquist plots of the ER, BRW/ER, PANI/ER, PANI@BRW/ER1, PANI @BRW/ER2, and PANI@BRW/ER3 coatings after 0 h (**a**,**b**), 72 h (**c**,**d**), and 168 h (**e**,**f**) immersion.

3.2.5. Adhesion Test

Adhesion is a key factor for a coating to maintain a long service life [39]. In this study, a digital pull-off instrument was used to evaluate the adhesion of coatings on the substrates. An aluminum dolly with a diameter of 20 mm was adhered to coatings with a binder and the pull-off test was performed after curing for 48 h. The adhesion was quantified as the force used to separate the coating from the metal substrate.

PANI@BRW/ER2, which performed better in the previous test, was selected for testing, and ER, BRW/ER, and PANI/ER were used as comparisons. Figure 12 shows the adhesion test results of all the coatings. The adhesion strength of the PANI@BRW/ER2 coating reached 7.86 MPa, while the adhesion strengths of the ER, BRW/ER, and PANI/ER coatings were 3.39, 5.47, and 4.16 MPa, respectively. This may result from the good dispersion and improved compatibility of PANI@BRW in epoxy resin [40].
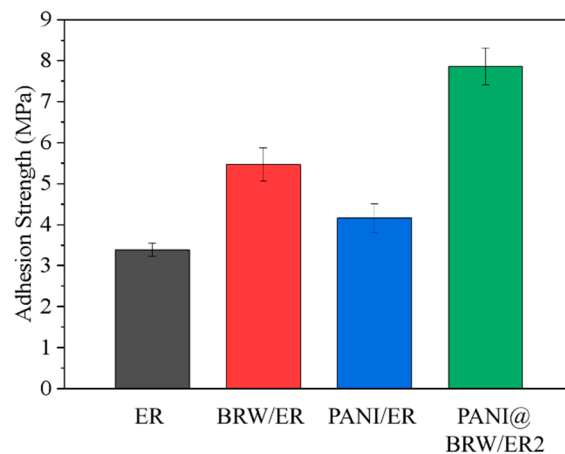
Figure 12. Adhesion strength results of ER, BRW/ER, PANI/ER, and PANI@BRW/ER2 coatings (the error bars show the standard error of the mean obtained from five repeated tests.

4. Conclusions

In this study, polyaniline-coated basalt rockwool waste (PANI@BRW) composites were prepared as fillers to serve in coatings for anti-corrosion applications. The results show that the modified BRW had better dispersion stability in some organic solvents, as well as compatibility with epoxy resin. Moreover, the salt spray test, OCP, polarization curve, and EIS measurements were adopted to evaluate the corrosion resistance of the coatings with PANI@BRW. The results indicate that the addition of PANI@BRW improved the anti-corrosion performance of the epoxy coatings. The coating containing 5% PANI@BRW exhibited the best anticorrosion performance with the highest protection efficiency (*PE*) of 97.7% and the highest impedance modulus ($|Z|_{0.01}$). Therefore, this study provides a potential application of basalt rockwool wastes as a new type of filler in the anti-corrosion coatings. This application is also expected to create considerable economic benefits in industry in the future.

Author Contributions: Conceptualization, G.W. and Z.F.; methodology, Z.F.; validation, Z.F., Y.Y., and L.H.; formal analysis, Z.F. and Y.X.; investigation, Z.F. and P.W.; resources, G.W.; data curation, Z.F.; writing—original draft preparation, Z.F. and J.L. (Jiang Li); writing—review and editing, G.W.; visualization, P.W.; supervision, G.W.; project administration, G.W. and J.L. (Jianhe Liao); funding acquisition, G.W. and A.W. All authors have read and agreed to the published version of the manuscript.

Institutional Review Board Statement: Not applicable.

Informed Consent Statement: Not applicable.

Data Availability Statement: Data is contained within the article.

Conflicts of Interest: The authors declare no conflict of interest.

References

1. Keerthan, P.; Mahendran, M. Thermal Performance of Composite Panels Under Fire Conditions Using Numerical Studies: Plasterboards, Rockwool, Glass Fibre and Cellulose Insulations. *Fire. Technol.* **2013**, *49*, 329–356. [CrossRef]
2. Rocha, E.; Sousa, A.; Furtado, C.J.P.T. Properties Investigation of novel nitrile rubber composites with rockwool fibers. *Polym. Test.* **2020**, *82*. [CrossRef]

3. Kinnunen, P.; Yliniemi, J.; Talling, B.; Illikainen, M. Rockwool waste in fly ash geopolymer composites. *J. Mater. Cycles. Waste.* **2017**, *19*, 1220–1227. [CrossRef]

4. He, P.; Wang, J.X.; Lu, F.Y.; Ma, Q.; Wang, Z. Synergistic effect of polyaniline grafted basalt plates for enhanced corrosion protective performance of epoxy coatings. *Prog. Org. Coat.* **2017**, *110*, 1–9. [CrossRef]

5. He, P.; Wang, J.X.; Ma, Q.; Lu, F.Y.; Wang, Z.; Wang, S.C. Protective property of epoxy coatings containing polyaniline and laminar basalt in neutral, alkaline, and acidic media. *Mater. Corros.* **2017**, *68*, 1355–1364. [CrossRef]

6. Liu, Y.; Wang, J.W.; Liu, L.; Li, Y.; Wang, F.H. Study of the failure mechanism of an epoxy coating system under high hydrostatic pressure. *Corros. Sci.* **2013**, *74*, 59–70. [CrossRef]

7. Cai, K.W.; Zuo, S.X.; Luo, S.P.; Yao, C.; Liu, W.J.; Ma, J.F.; Mao, H.H.; Li, Z.Y. Preparation of polyaniline/graphene composites with excellent anti-corrosion properties and their application in waterborne polyurethane anticorrosive coatings. *Rsc. Adv.* **2016**, *6*, 95965–95972. [CrossRef]

8. Dou, B.J.; Xiao, H.; Lin, X.Z.; Zhang, Y.J.; Zhao, S.X.; Duan, S.; Gao, X.L.; Fang, Z.W. Investigation of the Anti-Corrosion Properties of Fluorinated Graphene-Modified Waterborne Epoxy Coatings for Carbon Steel. *Coatings* **2021**, *11*, 254. [CrossRef]

9. Hao, Y.S.; Sani, L.A.; Ge, T.J.; Fang, Q.H. Phytic acid doped polyaniline containing epoxy coatings for corrosion protection of Q235 carbon steel. *Appl. Surf. Sci.* **2017**, *419*, 826–837. [CrossRef]

10. Armelin, E.; Aleman, C.; Iribarren, J.I. Anticorrosion performances of epoxy coatings modified with polyaniline: A comparison between the emeraldine base and salt forms. *Prog. Org. Coat.* **2009**, *65*, 88–93. [CrossRef]

11. Yang, S.Q.; Zhu, S.; Hong, R.Y. Graphene Oxide/Polyaniline Nanocomposites Used in Anticorrosive Coatings for Environmental Protection. *Coatings* **2020**, *10*, 1215. [CrossRef]

12. Wang, M.S.; Zhang, J.; Zhang, L.Z.; Li, J.Q.; Wang, W.J.; Yang, Z.L.; Zhang, L.; Wang, Y.X.; Chen, J.C.; Huang, Y.; et al. Graphene-like Vanadium Oxygen Hydrate (VOH) Nanosheets Intercalated and Exfoliated by Polyaniline (PANI) for Aqueous Zinc-Ion Batteries (ZIBs). *Acs. Appl. Mater. Inter.* **2020**, *12*, 31564–31574. [CrossRef] [PubMed]

13. Bohari, N.A.; Siddiquee, S.; Saallah, S.; Misson, M.; Arshad, S.E. Optimization and Analytical Behavior of Electrochemical Sensors Based on the Modification of Indium Tin Oxide (ITO) Using PANI/MWCNTs/AuNPs for Mercury Detection. *Sens. Basel.* **2020**, *20*, 6502. [CrossRef] [PubMed]

14. Liu, Y.; Lin, Z.; Lin, W.; Moon, K.S.; Wong, C.P. Reversible Superhydrophobic–Superhydrophilic Transition of ZnO Nanorod/Epoxy Composite Films. *Acs. Appl. Mater. Inter.* **2012**, *4*, 3959–3964. [CrossRef]

15. Hao, Y.S.; Zhao, Y.F.; Li, B.; Song, L.X.; Guo, Z. Self-healing effect of graphene@PANI loaded with benzotriazole for carbon steel. *Corros. Sci.* **2020**, *163*. [CrossRef]

16. Shetty, K.; Jayadev; Raj, K.; Mohan, N. Synthesis, characterization and corrosion studies of polyanailine (PANI)/ceriem dioxide(CeO2) nano composite. *Mater. Today Proc.* **2020**, *27*, 2158–2163. [CrossRef]

17. Grgur, B.N.; Gvozdenović, M.M.; Mišković-Stanković, V.B.; Kačarević-Popović, Z. Corrosion behavior and thermal stability of electrodeposited PANI/epoxy coating system on mild steel in sodium chloride solution. *Prog. Org. Coat.* **2006**, *56*, 214–219. [CrossRef]

18. Shi, S.E.; Zhao, Y.Y.; Zhang, Z.M.; Yu, L.M. Corrosion protection of a novel SiO$_2$@PANI coating for Q235 carbon steel. *Prog. Org. Coat.* **2019**, *132*, 227–234. [CrossRef]

19. Li, C.; Li, Y.; Wang, X.; Yuan, S.C.; Lin, D.; Zhu, Y.J.; Wang, H.Y. Synthesis of hydrophobic fluoro-substituted polyaniline filler for the long-term anti-corrosion performance enhancement of epoxy coatings. *Corros. Sci.* **2021**, *178*. [CrossRef]

20. Liao, G.F.; Li, Q.; Xu, Z.S. The chemical modification of polyaniline with enhanced properties: A review. *Prog. Org. Coat.* **2019**, *126*, 35–43. [CrossRef]

21. Wu, Y.P.; Zhu, S.F.; Shi, P.; Yan, B.J.; Cai, D.Z.; Zhang, Y.P. Corrosion behavior of Al film on uranium in salt spray test. *Rsc. Adv.* **2017**, *7*, 14981–14988. [CrossRef]

22. Sathiyanarayanan, S.; Azim, S.S.; Venkatachari, G.J.E.A. A new corrosion protection coating with polyaniline–TiO$_2$ composite for steel. *Electrochim. Acta* **2007**, *52*, 2068–2074. [CrossRef]

23. Eskizeybek, V.; Sari, F.; Gulce, H.; Gulce, A.; Avci, A. Preparation of the new polyaniline/ZnO nanocomposite and its photocatalytic activity for degradation of methylene blue and malachite green dyes under UV and natural sun lights irradiations. *Appl. Catal. B Environ.* **2012**, *119*, 197–206. [CrossRef]

24. Fan, W.; Wang, H.; Wang, C.; Liu, Z.; Zhu, Y.; Li, K. Epoxy coating capable of providing multi-component passive film for long-term anti-corrosion of steel. *Appl. Surf. Sci.* **2020**, *521*. [CrossRef]

25. Mostafaei, A.; Zolriasatein, A. Synthesis and characterization of conducting polyaniline nanocomposites containing ZnO nanorods. *Prog. Nat. Sci. Mater.* **2012**, *22*, 273–280. [CrossRef]

26. Hayatgheib, Y.; Ramezanzadeh, B.; Kardar, P.; Mandavian, M. A comparative study on fabrication of a highly effective corrosion protective system based on graphene oxide-polyaniline nanofibers/epoxy composite. *Corros. Sci.* **2018**, *133*, 358–373. [CrossRef]

27. Hao, Y.S.; Zhao, Y.F.; Yang, X.X.; Hu, B.; Ye, S.W.; Song, L.X.; Li, R.G. Self-healing epoxy coating loaded with phytic acid doped polyaniline nanofibers impregnated with benzotriazole for Q235 carbon steel. *Corros. Sci.* **2019**, *151*, 175–189. [CrossRef]

28. Caldona, E.B.; de Leon, A.C.; Pajarito, B.B.; Advincula, R.C. Novel anti-corrosion coatings from rubber-modified polybenzoxazine-based polyaniline composites. *Appl. Surf. Sci.* **2017**, *422*, 162–171. [CrossRef]

29. Motlatle, A.M.; Ray, S.S.; Scriba, M. Polyaniline-clay composite-containing epoxy coating with enhanced corrosion protection and mechanical properties. *Synth. Met.* **2018**, *245*, 102–110. [CrossRef]

30. Li, Y.; Wang, G.Q.; Guo, Z.H.; Wang, P.Q.; Wang, A.M. Preparation of Microcapsules Coating and the Study of Their Bionic Anti-Fouling Performance. *Materials* **2020**, *13*, 1669. [CrossRef] [PubMed]

31. Kumar, A.M.; Gasem, Z.M. Effect of functionalization of carbon nanotubes on mechanical and electrochemical behavior of polyaniline nanocomposite coatings. *Surf. Coat. Tech.* **2015**, *276*, 416–423. [CrossRef]

32. Narayanasamy, B.; Rajendran, S. Electropolymerized bilayer coatings of polyaniline and poly(N-methylaniline) on mild steel and their corrosion protection performance. *Prog. Org. Coat.* **2010**, *67*, 246–254. [CrossRef]

33. Tian, Z.F.; Yu, H.J.; Wang, L.; Saleem, M.; Ren, F.J.; Ren, P.F.; Chen, Y.S.; Sun, R.L.; Sun, Y.B.; Huang, L. Recent progress in the preparation of polyaniline nanostructures and their applications in anticorrosive coatings. *Rsc. Adv.* **2014**, *4*, 28195–28208. [CrossRef]

34. Ashassi-Sorkhabi, H.; Es'haghi, M. Corrosion protection of mild steel by nano-colloidal polyaniline/nanodiamond composite coating in NaCl solution. *J. Coat. Technol. Res.* **2014**, *11*, 371–380. [CrossRef]

35. Mostafaei, A.; Nasirpouri, F. Epoxy/polyaniline–ZnO nanorods hybrid nanocomposite coatings: Synthesis, characterization and corrosion protection performance of conducting paints. *Prog. Org. Coat.* **2014**, *77*, 146–159. [CrossRef]

36. Fan, L.L.; Miao, Z.X. Admittance-Based Stability Analysis: Bode Plots, Nyquist Diagrams or Eigenvalue Analysis? *IEEE T. Power. Syst.* **2020**, *35*, 3312–3315. [CrossRef]

37. Xu, Y.; Wang, S.; Peng, H.; Yang, Z.; Martin, D.J.; Bund, A.; Nanjundan, A.K.; Yamauchi, Y. Electrochemical Characteristics of Cobaltosic Oxide in Organic Electrolyte According to Bode Plots: Double-Layer Capacitance and Pseudocapacitance. *Chemelectrochem* **2019**, *6*, 2456–2463. [CrossRef]

38. Torknezhad, Y.; Khosravi, M.; Assefi, M. Corrosion protection performance of nanoparticle incorporated epoxy paint assessed by linear polarization and electrochemical impedance spectroscopy. *Mater. Corros.* **2018**, *69*, 472–480. [CrossRef]

39. Zhang, Y.J.; Shao, Y.W.; Zhang, T.; Meng, G.Z.; Wang, F.H. The effect of epoxy coating containing emeraldine base and hydrofluoric acid doped polyaniline on the corrosion protection of AZ91D magnesium alloy. *Corros. Sci.* **2011**, *53*, 3747–3755. [CrossRef]

40. Gupta, G.; Birbilis, N.; Cook, A.B.; Khanna, A.S. Polyaniline-lignosulfonate/epoxy coating for corrosion protection of AA2024-T3. *Corros. Sci.* **2013**, *67*, 256–267. [CrossRef]